ARTICLE

Estimating the Raman Cross Sections of Single Carbon Nanotubes

Johanna E. Bohn,[†] Pablo G. Etchegoin,[†,*] Eric C. Le Ru,[†] Rong Xiang,[‡] Shohei Chiashi,[‡] and Shigeo Maruyama[‡,*]

[†]The MacDiarmid Institute for Advanced Materials and Nanotechnology, School of Chemical and Physical Sciences, Victoria University of Wellington, P.O. Box 600, Wellington, New Zealand, and [‡]Department of Mechanical Engineering, The University of Tokyo, 7-3-1 Hongo, Bunkyo-ku, Tokyo, Japan

ABSTRACT The order of magnitude of Raman differential cross sections of radial breathing modes (RBMs) of individual carbon nanotubes is measured for 633 and 785 nm laser excitations. This is shown by both a calibration applied to previously published data from other authors at 785 nm and our own measurements of individual nanotubes at 633 nm excitation. We find typical values of differential cross sections of RBMs to be on the order of $\sim 10^{-22}$ cm^2/sr for resonant nanotubes on a silicon substrate. This study therefore provides a rigorous quantification of the accepted view that Raman cross sections of carbon nanotubes are "huge".

KEYWORDS: carbon nanotubes · radial breathing mode · SERS

The study of carbon nanotubes and related compounds has intensified in the past few years,[1−3] mainly driven by the prospects of using their unique electronic, mechanical, and optical properties in a variety of nanotechnology frameworks. Since the discovery of carbon nanotubes,[4] Raman spectroscopy[5] has played a leading role in our current understanding[6,7] and has led to the elucidation of a great variety of phenomena: from the characterization of nanotubes according to their radial breathing mode (RBM) frequencies[8] to the study of double-resonance phenomena,[9] or "anomalous" anti-Stokes spectra.[10] Studies have also been extended to the realms of surface-enhanced Raman spectroscopy (SERS).[11]

Notwithstanding, there are still very basic aspects of Raman scattering of carbon nanotubes that have *not* yet been explored. One such example is the experimental estimation of the *differential Raman scattering cross sections* ($d\sigma/d\Omega$) for differing Raman modes (radial breathing modes (RBMs), G-bands, D-bands, *etc.*) of different types of nanotubes (semiconducting or metallic; characterized by their chirality indices (n, m)[12]). While a considerable fraction of papers in the topic mention the apparent "huge resonant Raman cross sections" that nanotubes have, a direct attempt to quantify them—even with intrinsic experimental limitations—has not yet been provided in the literature. Hence, this paper is aimed directly at filling what we perceive as a gap in the literature, that is, a direct experimental estimation of differential Raman cross sections of nanotubes, together with the development of a practical protocol that can be followed subsequently by other authors to quantify their observations. The importance of having a reliable estimation of the differential Raman cross sections of nanotubes is, we believe, beyond doubt. This stems not only from the viewpoint that the $d\sigma/d\Omega$ values of nanotubes represent one of their fundamental physical properties but also, in addition, from the fact that a proper estimation of Raman differential cross sections might start closing the circle into a whole variety of related phenomena that have been already observed (like the anomalous magnitude of anti-Stokes spectra[8,10] or the possibility of vibrational pumping).

The main problem with the estimation of Raman differential cross sections in general is to know *how many molecules are contributing to the signal*. While this is not a major problem for measurements done in transparent liquids of known density and molecular weight, where we can clearly define how many molecules are producing the signal in the scattering volume, it is a daunting task in samples with more complicated characteristics (like forests of nanotubes,[13,14] for example), in particular, if resonance effects produce signals that come from a subpopulation of the molecules that are actually in the scattering volume. A non-uniform sample such as a forest of nanotubes on a substrate presents a challenging experimental problem simply because it is not easy to normalize the sig-

*Address correspondence to pablo.etchegoin@vuw.ac.nz, maruyama@photon.t.u-tokyo.ac.jp.

Received for review March 2, 2010 and accepted May 7, 2010.

Published online May 19, 2010. 10.1021/nn100425k

nal by the number of tubes that are contributing to it. The addition of resonance phenomena only exacerbates the problem. A similar situation occurs, in fact, in SERS, where the inhomogeneity of the enhancement factor makes it very difficult in general to estimate how many molecules are contributing to the signal.[15,16] In this case, there is normally no other option but to try to observe *one* molecule (nanotube) at a time.[17] In this latter situation, the difficulty of estimating how many molecules are producing the signal is replaced by the experimental difficulty of finding a way to ensure that, indeed, single molecules are being measured. To this we have to add the experimental limitation that the cross section itself (intrinsic or enhanced in the case of SERS) has to be large enough to make single molecule (nanotube) observation possible. Fortunately, nanotubes fall into this category, without a need for further enhancement of the cross section like SERS.

Nanotubes are unlike any other normal case of Raman cross section determination for other (smaller) molecules. The fact that some nanotubes can be *longer* than a typical laser spot size (~0.5−1 μm, at high magnifications in optical microscopes) is an indication of how unusual their case is. A few peculiarities of the nanotube problem that are relevant for the forthcoming discussion can be introduced at this stage:

- Nanotubes provide a natural spectroscopic fingerprint to decide single nanotube detection through their radial breathing modes (RBMs), which, for a specific nanotube, is a signature of its uniqueness among a certain inhomogeneous population of tubes. After ref 12, the measurement of individual RBMs in samples with a low surface coverage (within the area defined by the laser spot) provides a natural mechanism for the identification of single nanotubes. In short, the detection of individual nanotubes is ensured by the combination of (*i*) samples with low surface density of tubes and (*ii*) the additional "resonance selection" by which only tubes with certain characteristics can effectively couple to a particular laser excitation.
- The Raman signals of nanotubes are typically highly polarized.[18] However, exactly as in ref 12, we do not have an easy way of controlling the relative orientation of different nanotubes with respect to the incident polarization. Nanotubes are detected by spatial Raman mappings on a substrate (Si). An example of a Raman map is given in the Supporting Information. We therefore expect that the largest values of the differential cross sections obtained in single nanotubes will be (statistically speaking) representative of the largest component of the Raman tensor, that is, when it is aligned accidentally in the right direction. Experimentally obtained values for $d\sigma/d\Omega$ need to be understood in that context.
- A similar proviso holds for the *length* of the nanotube. We cannot easily measure the actual length and the exact spatial position on an individual nanotube within the laser spot (simultaneously with the Raman spectrum itself). Nanotubes are rather large "molecules" with varying lengths in the typical range of ~100−300 nm (according to our SEM images); others[12] have grown even larger nanotubes (~1 μm). If we had the same type of nanotubes (defined by the chirality indices (n, m)) in resonance with the laser under the microscope all the time, and in the same position and orientation with respect to the laser polarization, there will still be a spread of signals caused by their intrinsic variability in length. As with the previous point, experimentally obtained values have to be interpreted in that context. As we shall explain later, we perform experiments with the minimum laser spot size attainable (w_0) by using the highest possible magnification available to us (×100), and hence, the largest $d\sigma/d\Omega$ values observed can be used as representative of the longest tubes, which possibly span the full length of the spot size. In turn, this allows us potentially to define a *differential cross section per unit length* of the tubes (which is then an intrinsic property irrespective of their length).

Hence, except for the fact that part of the information is hidden in the statistical spread of signals, this is *not* a limitation to estimate the order of magnitude of an intrinsic $d\sigma/d\Omega$, and in fact, the maximum measured cross sections should be a reliable estimate of how big the differential cross section per unit length can actually be for a specific wavelength (*i.e.*, a specific resonance condition). For the rest of the study, we concentrate only on estimations of $d\sigma/d\Omega$ values for the particular case of RBMs.

Undoubtedly, an important breakthrough in the spectroscopy of carbon nanotubes came with the realization that *individual* nanotubes could be observed.[12] This automatically provides a recipe for the quantification of Raman cross sections. As pointed out before, the unequivocal signature of individual single-walled carbon nanotubes grown on a Si substrate could be observed through their different RBMs[12] (see Figure 1). It is then possible to obtain an estimation of single nanotube differential Raman cross sections if we add an additional calibration (provided in the present study). We shall show explicitly here how this procedure can be performed, before moving on to a more direct measurement on our own samples.

Figure 1 (adapted from ref 12) demonstrates the presence of individual nanotubes at different positions in the sample by observing the presence of distinct RBMs, in a similar fashion as the bianalyte method used for single molecule detection in SERS.[19] The particular three individual nanotubes in Figure 1 have been

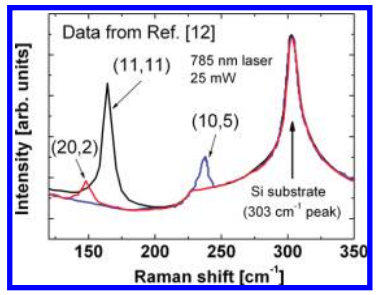

Figure 1. Individual single-walled carbon nanotube data (data reproduced from Figure 2 in ref 12). According to ref 12, these data correspond to individual nanotubes with different chiralities (specified by the numbers: (*n*, *m*) = (20,2), (11,11), and (10,5)). The spectra were taken on nanotubes grown by chemical vapor deposition on a Si substrate, with nanometer size iron catalyst particles (that act as a seed to start the growth). The sample had a density of ~6 nanotubes/μm^2, and the Raman spectra were taken with a 785 nm laser (1 μm^2 spot size, 25 mW laser power; see ref 12 for further details). The second-order Raman peak of Si at ~303 cm^{-1} is readily observable in the data and links to our calibration of Raman differential cross sections (see the Supporting Information).

labeled by their different chiralities (specified by the numbers (*n*, *m*) = (20,2), (11,11), and (10,5), after ref 12). These measurements have been performed in air, using a 785 nm laser with 25 mW (spot size ~1 μm^2). Each of the peaks gives an effective differential cross section for each individual tube. The trick is to link these values to a compound with a known differential cross section. For these particular results, this can be achieved using the second-order Raman peak of Si at ~303 cm^{-1} as a common reference. This Raman peak is *fully symmetric* (belonging to the Γ_1 irreducible representation of the point group of the crystal[20]), and hence, this minimizes potential problems with the polarization dependence of the signal according to the exact crystal orientation with respect to the incident polarization. This calibration requires a comparison of the Si Raman signal with a Raman cross section standard (nitrogen gas here) and a careful characterization of the scattering volume. This procedure is detailed in section S1 of the Supporting Information. The results for the three RBMs in Figure 1 from the data in ref 12 are summarized in Table 1. Single nanotube differential Raman cross sections range from 3 × 10^{-23} to 3 × 10^{-22} cm^2/sr (depending on the specific nanotube).

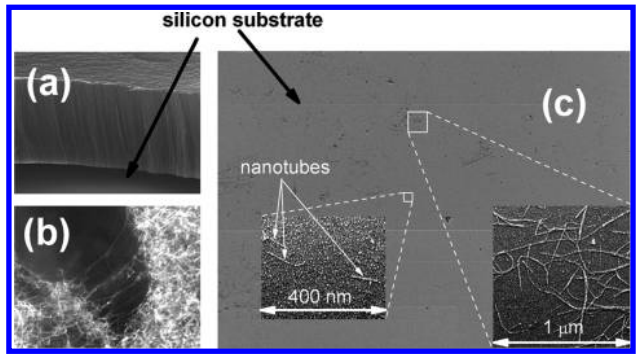

Figure 2. (a) Lateral SEM view of a forest of ^{13}C nanotubes on a Si substrate.[13,14] The tubes raise above the substrate to a height of ~20 μm. (b) Closer look at much higher magnification (×50K) reveals a dense mat of entangled tubes. The dark "gap" in the figure is ~100 nm accross. (c) General overview of the sample with dried nanotubes on Si (after dispersion, drying on Si, and repeated washings with water and ethanol). The two blown-up regions show multiple nanotubes (on the right) and isolated ones (on the left). Our final samples for Raman consist of regions of medium densities of tubes (~30−50 nanotubes/μm^2) and regions of much smaller densities (~0−5 nanotubes/μm^2). Undoubtedly, some parts of the sample still contain bundles of tubes, but many regions contain objects that can be classified as *single tubes* (as far as the resolution of SEM allows). There is an additional "filter" in the number of tubes that are selected to be seen in the Raman spectra at each point, that is, the resonance condition with the laser (633 nm). This reduces further the effective number of tubes that are observable within the laser spot (beam waist of ~450 nm; see Figure S2 in the Supporting Information). Typical Raman spectra taken on this sample are shown in Figure 3.

TABLE 1. Summary of the RBM Differential Raman Cross Sections Inferred from Data of Reference 12

(*n*,*m*)	(20,2)	(11,11)	(10,5)
dσ/dΩ (cm^2/sr)	3.28 × 10^{-23}	2.7 × 10^{-22}	4.1 × 10^{-23}

Obviously, this two-step estimation *via* an intermediate reference (the Si Raman peak) is not the best method, but it demonstrates how Raman cross sections may be estimated from existing nanotube data. We now describe a more direct measurement where Raman signals from individual nanotubes are directly compared to a Raman standard. For practical reasons, these experiments were carried out in slightly different samples (isotopically edited nanotubes) and at a different wavelength (633 nm). Details of the nanotube fabrication and sample preparation are given in section S2 of the Supporting Information. Examples of SEM images of our samples at different stages are shown in Figure 2. In the final samples for Raman, some regions contain clear evidence of multibranched structures which are obviously bundles not fully separated in the centrifugation process, while other "sparser" areas show clear evidence for smaller (isolated) straight tubular structures of ~100−300 nm in length, attributed to individual nanotubes. SEM is (unfortunately) incapable of resolving the real diameter of these structures to confirm that they are individual nanotubes, but this is where the selectivity of RBMs in Raman spectroscopy comes into play. Note that even if some of the small nanotube segments still contain some small degree of bundling, the additional selectivity provided by the Raman resonance with specific tubes makes the selection of "single cases" possible. Bundling might perturb slightly the effective differential cross section of an individual tube, but this is already contained within the dispersion of cases that we obtain in the Raman data (*vide infra*).

We performed Raman mappings with a 633 nm laser (3 mW) in a Jobin-Yvon LabRam spectrometer attached to a BX41 Olympus optical microscope with a 100× objective (indexed matched to air, NA = 0.9). The differential cross sections for this laser line are going to be calibrated with respect to the differential cross section of the ~2331 cm^{-1} mode of nitrogen gas (in air) at 633 nm. The results of the scattering volume charac-

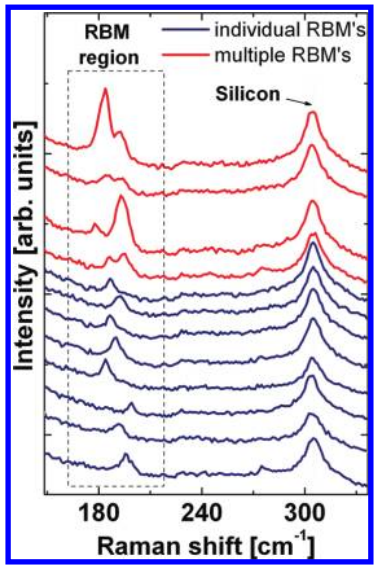

Figure 3. Selected spectra (out of 3 maps with 40 × 40 spectra) showing the unequivocal presence of RBMs corresponding to individual nanotubes. The spectra were taken with 3 mW at 633 nm and 10 s integration time with the 100× objective. We scan areas on the sample that look mostly "clean" from the perspective of an optical microscope with a 100× objective. Those areas are the ones that show the largest chance of detecting individual RBMs. Most of the time, the signal is simply that of the substrate. For these (isotopically edited) nanotubes, the RBM region is shown in a "box" in the figure. We show several examples of RBMs with different frequencies (blue), and we also show the presence of (every so often) spectra containing more than one type of RBM (red).

terization are summarized in Figure S2 of the Supporting Information. In Figure 3, we show several spectra selected from three different maps with 40 × 40 points (separated by 1 μm each (4800 spectra in total)). We found approximately ~70 clear cases of spectra with single RBMs (with frequencies fluctuating in the RBM region for this tubes; ~160−210 cm^{-1}) and ~100 clear events with multiple nanotubes. A few examples of both cases are shown in Figure 3. The RBMs that are singled out as coming from individual nanotubes (blue spectra in Figure 3) can be directly compared with the nitrogen calibration differential cross section in Figure S2 (accounting for the difference in integration times, while the power is kept constant at 3 mW). The analysis of the statistics of single nanotube signals and their differential cross sections is presented in Figure 4. We obtain differential cross sections for RBMs in the range:

$$\left(\frac{d\sigma}{d\Omega}\right)_{RBMs}^{633nm} \sim 1-4 \times 10^{-22}\ cm^2/sr\ (on\ silicon) \quad (1)$$

With all the provisos in mind of the experimental limitations to the (normally very difficult) problem of estimating $d\sigma/d\Omega$ values, we can conclude that the experimental determination of differential cross sections for single nanotubes is indeed possible. Moreover, the two results from the two completely independent experiments can be considered to be in good agreement within experimental errors. Small differences can arise for a variety of reasons. For a start, the tubes in ref 12 are

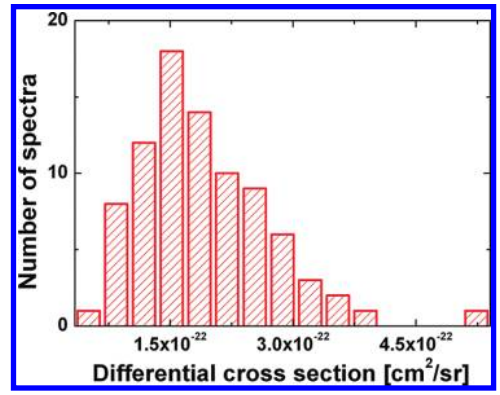

Figure 4. Histogram of differential Raman cross sections of individual RBMs of single nanotubes on Si from our Raman maps.

not the same type of tubes as we are measuring in our sample, and they are possibly larger (on average) than ours. In addition, there could be both a different resonance condition at 785 nm (expected) and an inaccurate estimation of the spot size (which was not the main point in ref 12, and therefore, it is not estimated through a beam profiling method, like we do in the Supporting Information of this paper). One way or another, we believe that both results show a consistent estimation of resonant differential cross sections in the range 4×10^{-23} to 4×10^{-22} cm^2/sr, both at 633 and 785 nm excitation. It should be noted that these values apply to those nanotubes that were most resonant with the laser excitation, among a larger population.

Moreover, these values relate to the special case of *nanotubes on silicon*. If the same tubes were measured in vacuum or in a solvent, some corrections would arise. First, the Si/air interface modifies the local electromagnetic environment, thereby affecting the Raman cross section. This is the equivalent of the *enhancement factor* of SERS[16] and can be estimated in a first approximation from the Fresnel coefficients of the Si/air interface to be $F \sim (4/(n+1)^2)^2$, where n is the refractive index of Si. At 633 or 785 nm (where $n \sim 4$, mostly real[21]), it results in an enhancement factor correction on Si of $F \sim 0.0064$; that is, the cross section on Si should be approximately 150 times smaller than the one in vacuum (silicon actually *quenches* the Raman signal). In a solvent, a local field correction should also be applied.[16] For example, in water, the Raman cross section is expected to be ~2.5 larger than that in vacuum.[16] Applying these corrections, we can predict Raman cross sections on the order of $\sim 10^{-20}$ cm^2/sr for RBM of the most resonant nanotubes in water. Finally, there may also be some chemical interaction of the nanotubes with the Si surface, which affects its electronic resonance and/or its Raman polarizability. Such effects are however difficult to quantify theoretically.

A natural question at this point is: how do these values compare with known differential cross sections of smaller resonant molecules? Although measuring resonant cross sections in dyes is a difficult task in general, the largest estimates of resonant differential resonant

Raman cross sections are of the order of $\sim 10^{-24}$ cm^2/sr (*e.g.*, for rhodamine 6G[22] in resonance at 532 nm laser excitation). Raman cross sections of resonant nanotubes on Si are therefore a factor ~100 larger than those of resonant dyes (and possibly as much as ~1000 larger for nanotubes in water). These estimates should be useful for further theoretical investigations of the physical origin of the large Raman cross section of carbon nanotubes.

Finally, the large Raman cross section of carbon nanotubes goes some ways in explaining why *single* carbon nanotubes can be detected by Raman spectroscopy. However, their cross section remains smaller than typical SERS cross sections required for single molecule detection of dyes with SERS.[16,17,23] The fact that they are "more visible" using Raman (with respect to resonant dyes) comes from the combination of two main factors: (*i*) they do not have problems with fluorescence, and (*ii*) they are incredibly robust against photobleaching (comparatively speaking), therefore allowing us to use long integration times and large laser power densities. No resonant dye would survive for an integration time of 10 s with 3 mW of 633 nm laser under a 100× objective, as in Figure 3. Therefore, the detection of single dyes is considerably more difficult and needs to resort to additional amplification (*i.e.*, SERS).

An important point of this study is that it rigorously quantifies the common view that resonant Raman cross sections of carbon nanotubes are "huge". We believe a proper estimation of the order of magnitude of differential cross sections of single nanotubes will contribute to the general understanding of the field and will help to elucidate the real origin of other phenomena (that depend on the magnitude of the cross section) that has so far remained elusive in nanotubes, such as vibrational pumping.

Acknowledgment. We are indebted to Shrividya Ravi and Chris Bumby (Victoria University of Wellington) for useful discussions and help with some of the samples. Special thanks are given to A. Pantoja (Beaglehole Instruments, Wellington, NZ) for lending us a calibration lamp to test the response of our system.

Supporting Information Available: Details of the scattering volume characterization at 633 and 785 nm; method for using the apparent cross section of the 303 cm^{-1} mode of Si to determine the Raman cross section from published data; and further details on carbon nanotubes and sample preparation. This material is available free of charge *via* the Internet at http://pubs.acs.org.

REFERENCES AND NOTES

1. Reich, S.; Thomsen, C.; Maultzsch, J. *Carbon Nanotubes: Basic Concepts and Physical Properties*; Wiley-VCH: Berlin, 2004.
2. Saito, R. *Physical Properties of Carbon Nanotubes*; World Scientific: Singapore, 2004.
3. Jorio, A., Dresselhaus, G., Dresselhaus, M. S., Eds. *Carbon Nanotubes: Advanced Topics in the Synthesis, Structure, Properties and Applications*; Springer: Berlin, 2008.
4. Iijima, S. Helical Microtubules of Graphitic Carbon. *Nature* **1991**, *354*, 56–58.
5. Long, D. A. *The Raman Effect, A Unified Treatment of the Theory of Raman Scattering by Molecules*; John Wiley & Sons Ltd.: Chichester, UK, 2002.
6. Dresselhaus, M. S.; Pimenta, M. A.; Kneipp, K.; Brown, S. D. M.; Corio, P.; Marucci, A.; Dresselhaus, G. *Science and Applications of Nanotubes*; Kluwer Academic/Plenum Publishers: New York, 2000.
7. Lefrant, S.; Buisson, J.; Schreiber, J.; Wery, J.; Faulques, E.; Chauvet, O.; Baibarac, M.; Baltog, I. *Spectroscopy of Emerging Materials*; Kluwer Academic Publishers: Amsterdam, 2004.
8. Dresselhaus, M. S.; Eklund, P. C. Phonons in Carbon Nanotubes. *Adv. Phys.* **2000**, *49*, 705–814.
9. Saito, R.; Grüneis, A.; Samsonidze, G. G.; Brar, V. W.; Dresselhaus, G.; Dresselhaus, M. S.; Jorio, A.; Cancado, L. G.; Fantini, C.; Pimenta, M. A.; Filho, A. G. S. Double Resonance Raman Spectroscopy of Single-Wall Carbon Nanotubes. *New J. Phys.* **2003**, *5*, 157.1157.15.
10. Filho, A. G. S.; Chou, S. G.; Samsonidze, G. G.; Dresselhaus, G.; Dresselhaus, M. S.; An, L.; Liu, J.; Swan, A. K.; Ünlü, M. S.; Goldberg, B. B.; Jorio, A.; Grüneis, A.; Saito, R. Stokes and Anti-Stokes Raman Spectra of Small-Diameter Isolated Carbon Nanotubes. *Phys. Rev. B* **2004**, *69*, 115428-1–115428-8.
11. Kneipp, K.; Kneipp, H.; Dresselhaus, M. S.; Lefrant, S. Surface-Enhanced Raman Scattering on Single Wall Carbon Nanotubes. *Philos. Trans. R. Soc. London, Ser. A* **2004**, *362*, 2361–2373.
12. Jorio, A.; Saito, R.; Hafner, J. H.; Lieber, C. M.; Hunter, M.; McClure, T.; Dresselhaus, G.; Dresselhaus, M. S. Structural (*n*,*m*) Determination of Isolated Single-Wall Carbon Nanotubes by Resonant Raman Scattering. *Phys. Rev. Lett.* **2001**, *86*, 1118–1121.
13. Murakami, Y.; Chiashi, S.; Miyauchi, Y.; Hu, M.; Ogura, M.; Okubo, T.; Maruyama, S. Growth of Vertically Aligned Single-Walled Carbon Nanotube Film on Quartz Substrates and Its Optical Anisotropy. *Chem. Phys. Lett.* **2004**, *385*, 298–303.
14. Xiang, R.; Zhang, Z.; Ogura, K.; Okawa, J.; Einarsson, E.; Miyauchi, Y.; Shiomi, J.; Maruyama, S. Vertically Aligned ^{13}C Single-Walled Carbon Nanotubes Synthesized by No-Flow Alcohol Chemical Vapor Deposition and Their Root Growth Mechanism. *Jpn. J. Appl. Phys.* **2008**, *47*, 1971–1974.
15. Le Ru, E. C.; Etchegoin, P. G.; Meyer, M. Enhancement Factor Distribution around a Single Surface-Enhanced Raman Scattering Hot Spot and Its Relation to Single Molecule Detection. *J. Chem. Phys.* **2006**, *125*, 204701-1–204701-13.
16. Le Ru, E. C.; Etchegoin, P. G. *Principles of Surface Enhanced Raman Spectroscopy and Related Plasmonic Effects*; Elsevier: Amsterdam, 2009.
17. Le Ru, E. C.; Blackie, E.; Meyer, M.; Etchegoin, P. G. Surface Enhanced Raman Scattering Enhancement Factors: A Comprehensive Study. *J. Chem. Phys. C* **2007**, *111*, 13794–13803.
18. Duesberg, G. S.; Loa, I.; Burghard, M.; Syassen, K.; Roth, S. Polarized Raman Spectroscopy on Isolated Single-Wall Carbon Nanotubes. *Phys. Rev. Lett.* **2000**, *85*, 5436–5439.
19. Le Ru, E. C.; Meyer, M.; Etchegoin, P. G. Proof of Single-Molecule Sensitivity in Surface Enhanced Raman Scattering (SERS) by Means of a Two-Analyte Technique. *J. Phys. Chem. B* **2006**, *110*, 1944–1948.
20. Yu, P. Y.; Cardona, M. *Fundamentals of Semiconductors: Physics and Materials Properties*; Springer: Berlin, 2004.
21. Etchegoin, P. G.; Kircher, J.; Cardona, M. Elasto-optical Constants of Si. *Phys. Rev. B* **1992**, *47*, 10292–10303.
22. Shim, S.; Stuart, C. M.; Mathies, R. A. Resonance Raman Cross-Sections and Vibronic Analysis of Rhodamine 6G from Broadband Stimulated Raman Spectroscopy. *ChemPhysChem* **2008**, *9*, 697–699.
23. Etchegoin, P. G.; Le Ru, E. C. A Perspective on Single Molecule SERS: Current Status and Future Challenges. *Phys. Chem. Chem. Phys.* **2008**, *10*, 6079–6089.

Supplementary information for "Estimating the Raman cross sections of single carbon nanotubes", by *Johanna E. Bohn, Pablo G. Etchegoin, Eric C. Le Ru, Rong Xiang, Shohei Chiashi, and Shigeo Maruyama*

SECTION S1: CALIBRATION METHOD: SCATTERING VOLUME CHARACTERIZATION AND APPARENT CROSS SECTION OF SILICON

Hereafter, we explain how an apparent Raman cross-section for the $303\,\mathrm{cm}^{-1}$ mode of Si was measured and then used to infer the nanotube Raman cross-sections from the previously published data in Ref. 1 at 785 nm. We start by discussing the scattering volume characterization, which is also needed for a direct measurement of the nanotube Raman cross-section at 633 nm as discussed in the main text.

Scattering volume characterization

It is easier (for experimental reasons) to start with a substance with known differential cross section that can be measured in a *volume* (typically a liquid or a gas) rather than on a surface. This is because it is easier in this former case to estimate the number of molecules contributing to the signal (given the density and molecular weight of the substance). Henceforth, this implies the previous knowledge and characterization of the scattering volume, which is shown for our ×100 objective (air) in Figures S1 (at 785 nm) and S2 (at 633 nm).

The scattering volume characterization is done by measuring first the *beam waist* (w_0), using the confocal pinhole and relating this value to the actual waist of the beam on the image plane through the magnification of the collecting optics. This is schematically shown in Fig. S1(a). Furthermore, it is necessary to determine the *depth of focus* (H_{eff}) in the axial direction, shown in Fig. S1(b). The full characterization of the scattering volume has been described in detail in the supplementary information of Ref. 2 and, therefore, it will not be repeated here. We only concentrate on a summary of the results in the following points:

- From the data at 785 nm in Fig. S1(a) (using the nomenclature and methods of Ref. 2) we obtain $w_0 = 1.2\,\mu$m, while the profile in the axial direction in Fig. S1(b) gives the effective depth of focus of $H_{\mathrm{eff}} = 19\,\mu$m. From here we obtain an effective scattering volume of $V_{\mathrm{eff}}^{785\,\mathrm{nm}} = (\pi/2) w_0^2 H_{\mathrm{eff}} = 43.0\,\mu\mathrm{m}^3$ at 785 nm laser excitation with an effective spot area of $A_{\mathrm{eff}}^{785\,\mathrm{nm}} = 2.26\,\mu\mathrm{m}^2$.

- As a calibration Raman standard for differential cross sections, we use the nitrogen gas in air at normal atmospheric conditions. We can calculate the effective number of molecules (N) contained in the scattering volume from the partial pressure of nitrogen (78%): $N = 8.1\,10^8$ molecules.

- With N known, we can take the differential Raman cross section per molecule of N_2 (for the only vibration at $2331\,\mathrm{cm}^{-1}$, with $d\sigma/d\Omega = 7 \times 10^{-32}\,\mathrm{cm}^2/\mathrm{sr}$ at 785 nm) and write down an expression for the signal measured by the spectrometer as:

$$I_{\mathrm{N_2}} = \alpha\rho\tau N \cdot \left(\frac{d\sigma}{d\Omega}\right)_{\mathrm{N_2}}^{785\,\mathrm{nm}}, \qquad \text{(S1)}$$

  where the signal $I_{\mathrm{N_2}}$ is measured in counts, ρ is the power density [W/m^2], τ [sec] the integration time, and α is a fixed factor accounting for the overall collection efficiency. The actual signal of N_2 under the experimental conditions we are using ($650\,\mu$W @ 785 nm, 300 sec integration time, ×100 objective) is shown explicitly in Fig. S1(c).

A similar characterization is carried out at 633 nm for the direct measurement of single nanotube cross-sections. The beam-waist (w_0) measurement (in Fig. S2(a)) with the confocal pinhole of our microscope rendered a value of $w_0 = 450\,$nm, which combined with the axial effective depth of focus [2] of $H_{\mathrm{eff}} = 16.5\,\mu$m (in Fig. S2(b)) gives an effective scattering volume of $V_{\mathrm{eff}} = 5.25\,\mu\mathrm{m}^3$. For air at normal pressure and temperature this results in $N \approx 10^8$ nitrogen molecules contributing to the Raman signal. The differential Raman cross-section of N_2 at 633 nm is $(d\sigma/d\Omega)_{\mathrm{N_2}}^{633\,\mathrm{nm}} = 16 \times 10^{-32}\,\mathrm{cm}^2/\mathrm{sr}$ [3] (note that the cross section of N_2 changes with excitation wavelength due to the well known ω^4-dependence of cross sections for non-resonant molecules). We conclude that the peak in Fig. S2(c) (obtained with 300 sec integration time) is equivalent to an effective differential cross section of: $(d\sigma/d\Omega)_{\mathrm{N_2}}^{\mathrm{eff}} = N \times (d\sigma/d\Omega)_{\mathrm{N_2}}^{633\,\mathrm{nm}} = 1.6 \times 10^{-23}\,\mathrm{cm}^2/\mathrm{sr}$.

Finally, in order to use this calibration to determine the RBM's Raman cross-sections, we also need to correct for the difference in the system response between $2331\,\mathrm{cm}^{-1}$ (nitrogen) and $\sim 200\,\mathrm{cm}^{-1}$ (RBM's) at 633 nm excitation. This difference in response is a factor of 1.45 in our system (measured again against a calibrated lamp).

Apparent Si cross-section

Once the scattering volume has been fully characterized, an apparent Si cross-section can be defined and determined as follows. Under the same experimental conditions (power, integration time, numerical aperture of the

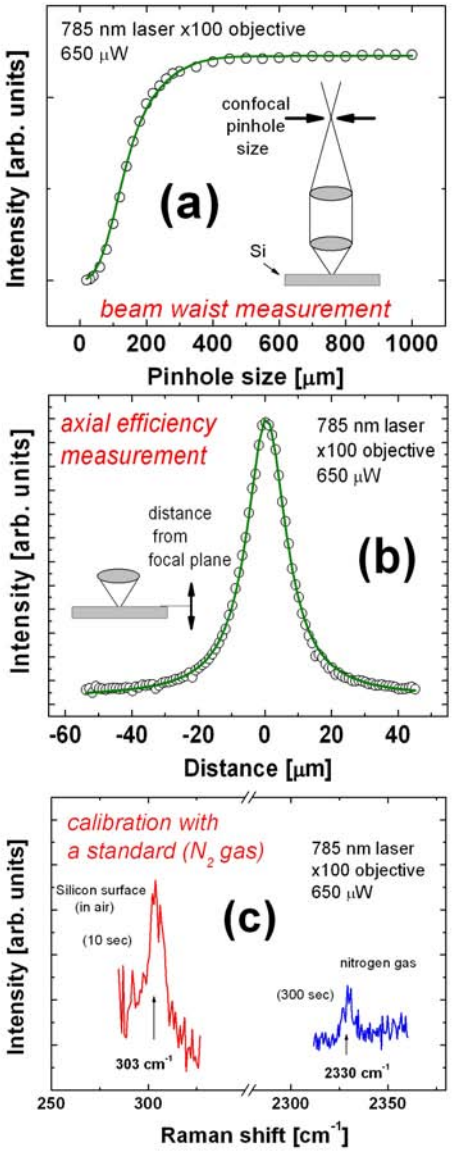

FIG. S1: Characterization of the scattering volume of the microscope (see the supplementary information in Ref. 2 for an in-depth description of the procedure). The beam waist is measured in (*a*) by studying the pinhole size dependence of the intensity of the 520 cm^{-1} Raman peak of Si at the confocal plane (through the magnification of the collecting optics, which for our system is a factor of 56). The solid line shows the fit to the data following Ref. 2. In (*b*) the axial signal dependence is measured with the confocal pinhole fully opened, to define the *effective depth of focus*. This is done by measuring the signal for different positions of the sample with respect to the focal plane. The line in (b) is a guide to the eye; the actual confocal depth is calculated with Eq. S33 in Ref. 2. The data in (*b*) and the beam waist from (*a*) define the effective scattering volume [2]. In (*c*), a reference sample with a known Raman differential cross section (nitrogen gas) is measured in the scattering volume. The signal is then compared (with a normalization to account for the system response at different wavelengths) to the 303 cm^{-1} peak of Si to define an apparent cross section. This can then be used to quantify the differential cross sections of individual nanotubes from Ref. 1.

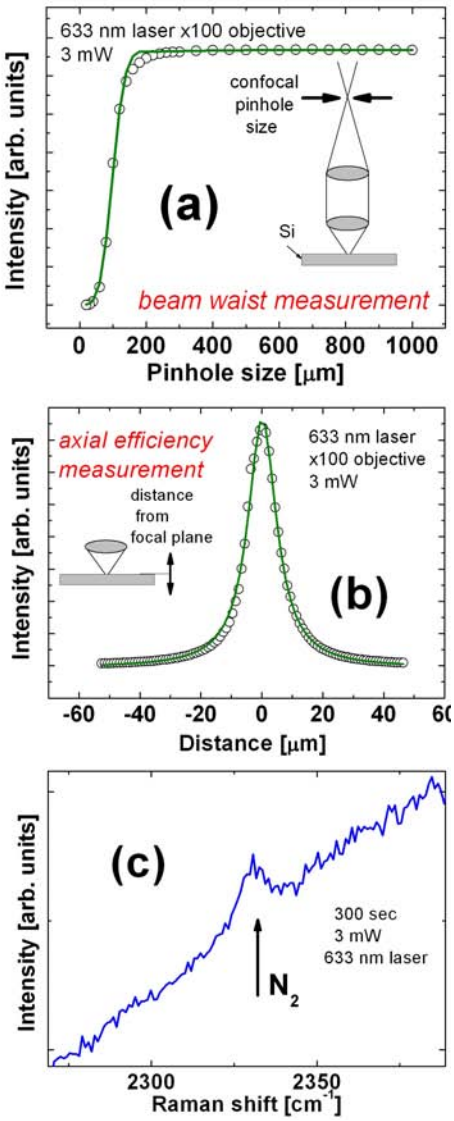

FIG. S2: (a) Beam waist and (b) axial efficiency characterizations of the scattering volume for the 633 nm laser with a ×100 objective (indexed matched to air). The combination of the results in (a) and (b) rendered a beam waist of $w_0 = 450\,\mathrm{nm}$, an effective depth of focus of $H_{\mathrm{eff}} = 16.5\,\mu\mathrm{m}$ (from Eq. S33 in Ref. 2), and an effective scattering volume V_{eff} of $5.25\,\mu\mathrm{m}^3$. (c) Nitrogen gas (in air) Raman signal at normal pressure and temperature. This signal is equivalent to an effective differential cross section of $1.6 \times 10^{-23}\,\mathrm{cm}^2/\mathrm{sr}$ and has been obtained with 300 sec integration time. The signal in (c) (normalized by the difference in integration times) serves as a basis to quantify the individual RBM's in Fig. 3 of the main text.

collecting optics, etc), we can focus the laser on a Si substrate (in air) and obtain the signal of the second-order (acoustic phonons) Raman peak of Si at $\sim 303\,\mathrm{cm}^{-1}$; this is also shown in Fig. S1(c). The ratio of integrated intensities with respect to the nitrogen signal allows us to define an *apparent* differential cross section per unit area

for this feature at a Si/air interface. Note that *this is not the differential cross section*, which in a solid is normally given for crystals as a differential cross section per unit cell (or per atom) [4, 5]. The apparent differential cross section per unit area, on the contrary, is simply a value to link the intensity of this peak to a known standard. For as long as we use the same laser (*i.e.* the same penetration depth) in another experiment, we can link the intensity of this feature in Si to a known standard through the definition of the apparent cross section per unit area. For the signal on the Si substrate we define:

$$I_{\mathrm{Si}}^{(1)} = \alpha\rho\tau \cdot \frac{d\Sigma}{d\Omega} \cdot A^{(1)} \tag{S2}$$

$$\Longrightarrow \quad \frac{d\Sigma}{d\Omega} = \frac{I_{\mathrm{Si}}^{(1)}}{I_{\mathrm{N_2}}} \cdot \frac{N}{A^{(1)}} \cdot \left(\frac{d\sigma}{d\Omega}\right)_{\mathrm{N_2}}^{785\,\mathrm{nm}}, \tag{S3}$$

where $d\Sigma/d\Omega$ is the apparent cross section per unit area of the Si substrate (for the $\sim 303\,\mathrm{cm}^{-1}$ mode), $A^{(1)}$ is the laser spot area in this experiment; and ρ, τ, and α have the same meaning as before. Note that $d\Sigma/d\Omega$ is obtained through a ratio of intensities measured with the same spectrometer and, accordingly, it becomes independent of ρ and (more importantly) of α. Note also that $d\Sigma/d\Omega$ is an intrinsic property of Si at this wavelength and it has units of sr^{-1} (because it is a cross section per unit area). Last, but not least, $d\Sigma/d\Omega$ needs to be corrected by the response of the system; this is necessary because the $2331\,\mathrm{cm}^{-1}$ mode of nitrogen is far from the $303\,\mathrm{cm}^{-1}$ mode of Si and (in the NIR in particular) the system response might not the same. Our system detects 3.35 times more at $303\,\mathrm{cm}^{-1}$ than $2330\,\mathrm{cm}^{-1}$ (with respect to a 785 nm excitation), as measured by comparison with a calibrated halogen lamp of known effective emission (black-body) temperature (2700 K). With all factors taken into account we find:

$$\frac{d\Sigma}{d\Omega} = 5.43 \times 10^{-14}\,\mathrm{sr}^{-1} \qquad \text{at } 785\,\mathrm{nm} \tag{S4}$$

We now have all the elements to link the signals of RBM's from individual nanotubes to a known standard in experiments performed by others. If the area of the laser spot in somebody else's experiment at 785 nm is known, and the $303\,\mathrm{cm}^{-1}$ Si signal is visible, we can always deduce what the equivalent differential cross section of the latter is, and relate this (through a simple intensity ratio) to the signal of the RBM's of nanotubes in the same spectrum.

Explicitly, knowing the area of the laser spot in Ref. 1 ($A^{(2)} \sim 1\,\mu\mathrm{m}^2$), the Si signal can be expressed as:

$$I_{\mathrm{Si}}^{(2)} = \alpha_2\rho_2\tau_2 \cdot \frac{d\Sigma}{d\Omega} \cdot A^{(2)}, \tag{S5}$$

where ρ_2, τ_2, and α_2 are again the power density, integration time and internal system response (for this new experiment, which could be done in a completely different spectrometer), $A^{(2)}$ is the new laser spot area and $d\Sigma/d\Omega$ is the (intrinsic) cross section per unit area of the $303\,\mathrm{cm}^{-1}$ Si signal coming from our calibration in Eq. S3. On the other hand, the signal of a RBM of a single carbon nanotube in the same spectrum will be given by:

$$I_{\mathrm{SCNT}}^{\mathrm{RBM}} = \alpha_2\rho_2\tau_2 \cdot \left(\frac{d\sigma}{d\Omega}\right)_{\mathrm{RBM's}}^{785\,\mathrm{nm}}, \tag{S6}$$

from where (taking the intensity ratio with Eq. S5, and replacing the expression for $d\Sigma/d\Omega$) we obtain:

$$\left(\frac{d\sigma}{d\Omega}\right)_{\mathrm{RBM's}}^{785\,\mathrm{nm}} = \frac{I_{\mathrm{SWNT}}^{\mathrm{RBM}}}{I_{\mathrm{Si}}^{(2)}} \cdot \frac{d\Sigma}{d\Omega} \cdot A^{(2)}. \tag{S7}$$

From Ref. 1 a value of ($A^{(2)} \sim 1\,\mu\mathrm{m}^2$) was assumed, while $I_{\mathrm{SWNT}}^{\mathrm{RBM}}$ and $I_{\mathrm{Si}}^{(2)}$ were estimated from Fig. 2 of Ref. 1 (reproduced in Fig. 1 of the main text). The resulting RBM cross-sections are summarized in Table I of the main text.

SECTION S2: CARBON NANOTUBE AND SAMPLE PREPARATION

Vertically aligned ^{13}C single-wall nanotubes were synthesized at 850 °C using ethanol as a carbon source in a no-flow condition [6, 7]. This sample has been synthesized for a different purpose, but it turned out to be ideal for the determination of differential cross sections of single nanotubes. The isotopic substitution from ^{12}C to ^{13}C is of no consequence for this experiment, except for the fact that RBM frequencies appear at slightly smaller wavelengths. For the synthesis, Co/Mo binary metal particles were formed on a quartz substrate as the catalyst using dip-coating. The substrate was then annealed in air at 400 °C for 5 min before being heated to 850 °C under a 300 sccm (standard cubic centimeters per minute) Ar/H_2 flow (3% H_2, Ar balance) at a pressure of 40 kPa. Upon reaching the growth temperature, the chamber was evacuated. 1.3 kPa of ethanol was then introduced into the chamber to start the SWNT growth. To prepare a solution sample, the obtained SWNT film was scratched off the quartz and dispersed in D_2O with 0.5 wt% sodium dodecylbenzene sulfonate (NaDDBS) by a bath sonication for 30 min, followed by a horn sonication with an ultrasonic processor (Hielscher GmbH, UP-400S with H3/Micro-Tip 3) for 15 h at a power flux level of $\sim$300 W/cm^2. The solution is then dried on a clean Si wafer and subsequently dip-washed several times with both distilled water and ethanol (separately). The wafers look "almost clean" to the bare eye after repeated washing, but a closer look with Scanning Electron Microscopy (SEM) reveals isolated clusters of nanotubes strongly attached to the surface.

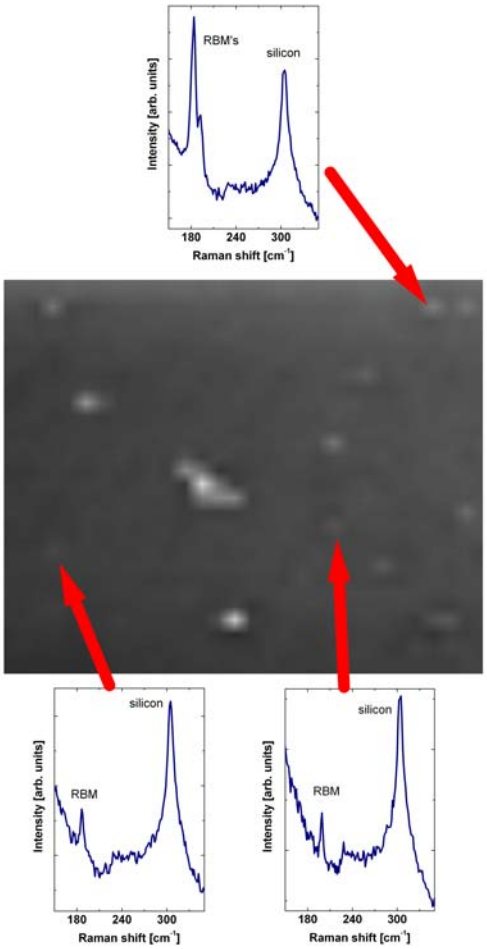

FIG. S3: A 40×40 (1μm spacing) Raman map at 633 nm (3 mW) and 10 sec integration time (see the main paper for further details on the experimental conditions). The map shows –in a black-white color scale– the integrated intensity of the spectrum in the RBM-fingerprint region ($\sim 150 - 220\,\mathrm{cm}^{-1}$). The "large" white islands represent regions with multiple (possibly entangled) tubes. Only the weakest isolated points in the map produce signals where only one RBM is present in the spectrum. A few of these isolated spots show sometimes evidence for more than one type of tube at the spot position. The spectrum at the top, for example, shows a case with two RBM's.

SECTION S3: RAMAN MAPS

Raman maps were taken (under the experimental conditions reported in the main paper) on 40×40 grids with points separated by 1 μm. Here we show an example of one of these maps. Most of the time, the signal is simply the spectrum of the substrate (Si). But in a few sparse places, signals with peaks in the fingerprint region of RBM's can be observed. In Fig. S3 we show a map where the integrated intensity in the RBM-region ($\sim 150 - 220\,\mathrm{cm}^{-1}$) is plotted as a function of position.

Several places in the map show evidence of "cluttering" of tubes with many different contributions from different RBM's. Only isolated (weaker) spots show evidence of signals coming from single tubes. Every so often it is possible to find isolated spots with signals from more than one tube (an example of which is shown at the top of Fig. S3). Two examples (at the bottom of Fig. S3) of single nanotube Raman signals with different RBM's are explicitly shown in the map. Only cases where the spectral purity of the RBM region is good enough to assign it to a single tube are used in the statistics of the differential cross sections shown in the paper (Fig. 4 of the main paper).

[1] A. Jorio, R. Saito, J. H. Hafner, C. M. Lieber, M. Hunter, T. McClure, G. Dresselhaus, and M. S. Dresselhaus, Phys. Rev. Lett. **86**, 1118 (2001).

[2] E. C. Le Ru, E. Blackie, M. Meyer, and P. G. Etchegoin, J. Chem. Phys. C **111**, 13794 (2007).

[3] E. C. Le Ru and P. G. Etchegoin, *Principles of Surface Enhanced Raman Spectroscopy and Related Plasmonic Effects* (Elsevier, Amsterdam, 2009).

[4] P. Y. Yu and M. Cardona, *Fundamentals of semiconductors: physics and materials properties* (Springer, Berlin, 2004).

[5] W. Hayes and R. Loudon, *Scattering of light by crystals* (Wiley, New York, 1975).

[6] Y. Murakami, S. Chiashi, Y. Miyauchi, M. Hu, M. Ogura, T. Okubo, and S. Maruyama, Chem. Phys. Lett. **385**, 298 (2004).

[7] R. Xiang, Z. Zhang, K. Ogura, J. Okawa, E. Einarsson, Y. Miyauchi, J. Shiomi, and S. Maruyama, Jpn. J. Appl. Phys. **47**, 1971 (2008).